Electronic Supplementary Material (ESI) for RSC Advances

Dielectric Properties of Polymethacrylate-Grafted Carbon Nanotube Composites

*Kenichi Hayashida**

Organic Materials Lab, Toyota Central R&D Labs., Inc.,
Nagakute, Aichi 480-1192, Japan

E-mail: e1440@mosk.tytlabs.co.jp

Supplementary Information

PCHMA-CNT samples.

The ATRP initiator-modified CNT (CNT-Br) was observed by transmission electron microscopy (TEM) (Fig. S1b). It is confirmed that an amorphous-like layer uniformly covers the CNT surface. The thickness of the layer is approximately 2 nm. Also, the grafted PCHMA chain is clearly observed in Fig. S1c. Table S1 summarizes the characteristics of the PCHMA-CNT samples, where PCHMA-CNT with Φ_{CNT} = 0.071 was newly synthesized in this study. The rest samples had been obtained at our previous study.[1]

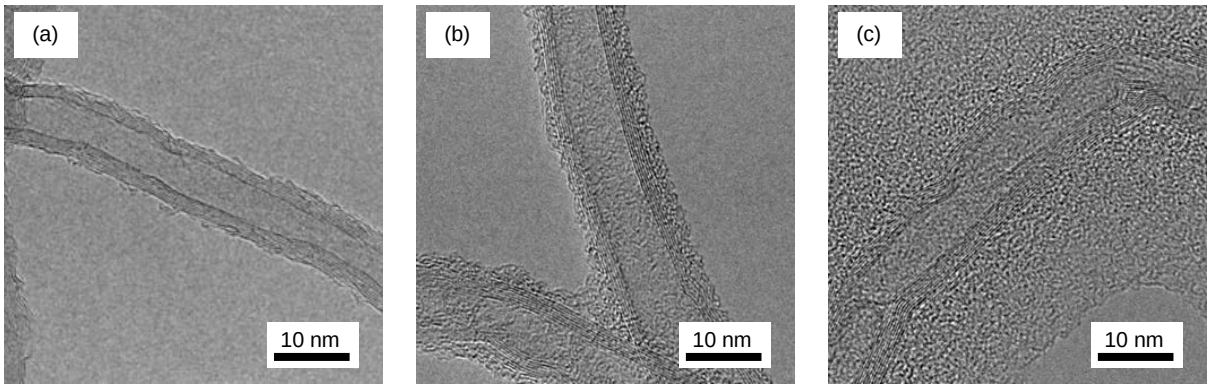

Fig. S1 TEM images of the modified CNTs: (a) CNT, (b) CNT-Br, (c) PCHMA-CNT.

Table S1 Characteristics of a Series of PCHMA-CNTs

$M_n \times 10^{-3}$ a)	fraction of CNT	
	Weight[b)]	Volume[c)]
60.2	0.214	0.143
72.5	0.188	0.124
82.5	0.171	0.112
102	0.145	0.094
143	0.111	0.071
190	0.087	0.055

[a)]Estimated using the loading amount (53 μmol g^{-1}) of the polymer chains on the CNT; [b)]Determined by the weight increment of the CNT sample after polymer-grafting; [c)]Calculated using a bulk density of 1.8 g cm^{-3} for the CNT and of 1.1 g cm^{-3} for the organic component.

1 K. Hayashida, H. Tanaka, *Adv. Funct. Mater.*, 2012, **22**, 2338.

SEM observation of PCHMA/CNT nanocomposites.

In the SEM observation, the surfaces of the nanocomposites that had been planed using an ultramicrotome, were slightly etched with oxygen plasma in order that the PCHMA polymer on the surface was removed out. Fig. S2 shows high resolution SEM images of PCHMA-CNT with Φ_{CNT} = 0.055 before and after the O_2 plasma etching. The individual CNTs can be clearly observed after the etching. Fig. S3 shows low magnification SEM images of the three types of nanocomposites with Φ_{CNT} = 0.055. The difference in dispersivity between these nanocomposites is distinctly recognized. PCHMA-CNT has excellent CNT dispersivity, while PCHMA/CNT-Br shows better dispersivity than PCHMA/CNT due to the improved polymer/CNT interface.

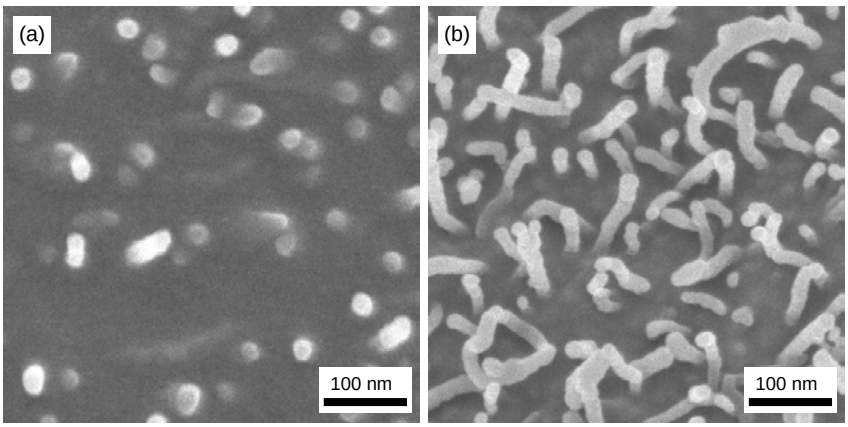

Fig. S2 High resolution SEM images of PCHMA-CNT with Φ_{CNT} = 0.055 (a) before and (b) after O_2 plasma etching.

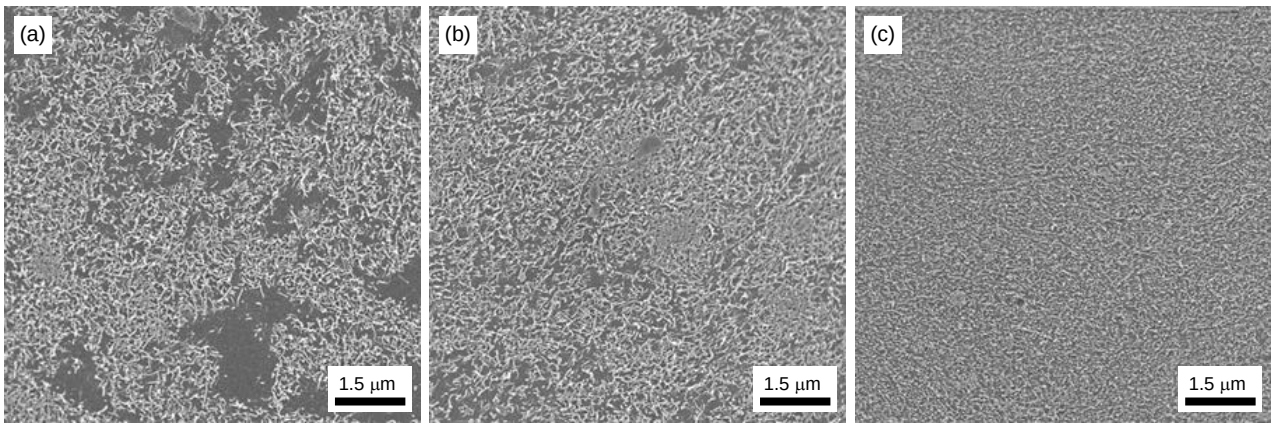

Fig. S3 Low magnification SEM images of three types of nanocomposites with Φ_{CNT} = 0.055: (a) PCHMA/CNT, (b) PCHMA/CNT-Br, (c) PCHMA-CNT.

Cole-Cole plots of the impedance spectra.

The R_s and X_s of impedance, $Z = R_s + jX_s$, is plotted as shown in Fig. S4. The Cole-Cole relaxation equation (eqn 2) is fitted to the Cole-Cole plot.

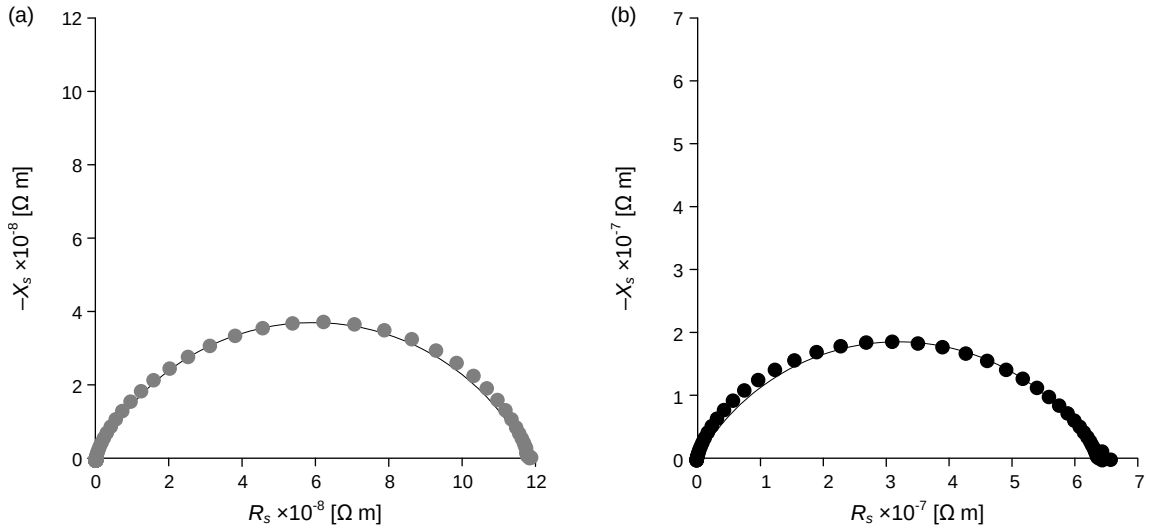

Fig. S4 Examples of Cole-Cole plots for two types of nanocomposites. (a) PCHMA/CNT-Br with Φ_{CNT} = 0.055. (b) PCHMA-CNT with Φ_{CNT} = 0.14. The solid line is a theoretical curve obtained from eqn (2).

Theoretical complex dielectric constant obtained from eqn (2).

From eqn (2), the reciprocal Z is expressed as;

$$1/Z = \{1+(j\omega/\omega_0)^{\beta}\}/R = \{1+(\omega/\omega_0)^{\beta}\cos(\pi\beta/2)\}/R + j\{(\omega/\omega_0)^{\beta}\sin(\pi\beta/2)\}/R.$$

Because $1/R_p = \varepsilon_0\omega\varepsilon_r''$ and $1/X_{cp} = -\varepsilon_0\omega\varepsilon_r'$, the following equations are obtained.

$$\varepsilon_r' = \sin(\pi\beta/2)/R\varepsilon_0\omega_0^{\beta}\omega^{1-\beta} + \varepsilon_r'_{\infty}, \quad (4)$$

$$\varepsilon_r'' = 1/R\varepsilon_0\omega + \cos(\pi\beta/2)/R\varepsilon_0\omega_0^{\beta}\omega^{1-\beta}, \quad (5)$$

where $\varepsilon_r'_{\infty}$ is the dielectric constant at infinite frequency. These theoretical curves of ε_r' and ε_r'' are consistent with the experimental results at the lower frequencies than ω_0 as shown in Fig. S5. At the higher frequencies than ω_0, however, eqns (4) and (5) are not consistent with the experimental spectra. This could be attributed to negligible tunneling conduction, because $-X_{cp}$ of the polymer bulk between the CNTs is lower than R_t at the higher frequencies than ω_0. Therefore, assuming that a parallel RC circuit is composed of a resistance R_B and a capacitance C for the polymer bulk (Fig. S7c), the following equations should be considered at the higher frequencies than ω_0.

$$\varepsilon_r' = \sin(\pi\beta/2)/R_B\varepsilon_0\omega_{0,b}^{\alpha}\omega^{1-\alpha} + \varepsilon_r'_{\infty}, \quad (S1)$$

$$\varepsilon_r'' = \cos(\pi\beta/2)/R_B\varepsilon_0\omega_{0,b}^{\alpha}\omega^{1-\alpha}, \quad (S2)$$

where $\omega_{0,b}$ is the relaxation frequency of the R_BC circuit. The exponent parameter α ($0 < \alpha \leq 1$) indicates stretching of the relaxation. According to our results, eqns (S1) and (S2) are well fitted to the experimental spectra at the higher frequencies than ω_0 as shown in Fig. S6 when $\alpha = \beta$.

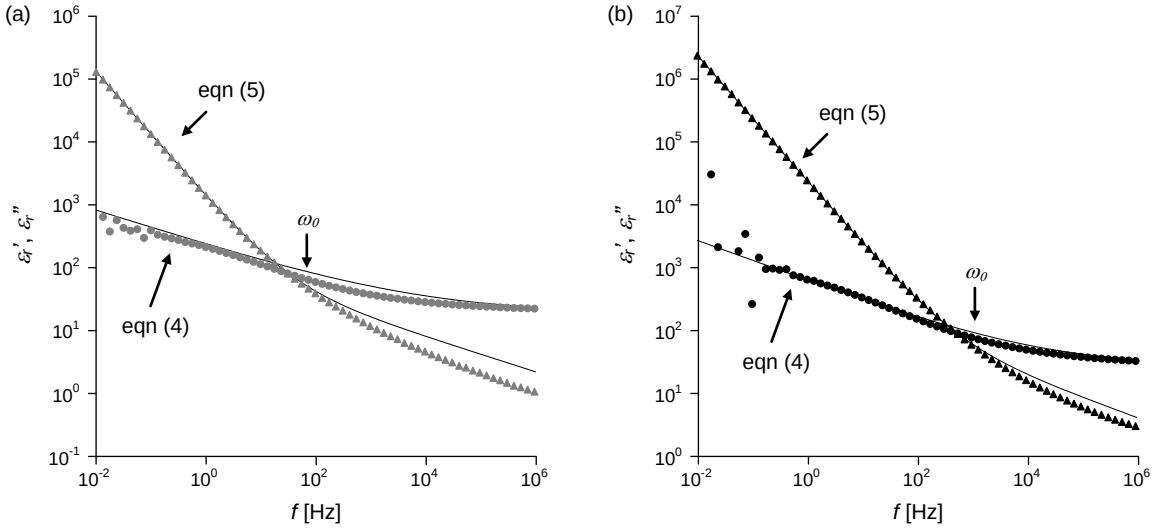

Fig. S5 Comparison between the experimental and theoretical spectra. (a) PCHMA/CNT-Br with Φ_{CNT} = 0.055. (b) PCHMA-CNT with Φ_{CNT} = 0.14. The solid lines are the theoretical curves, eqns (4) and (5) obtained from eqn (2) assuming that the Z relaxation related to the tunneling conduction.

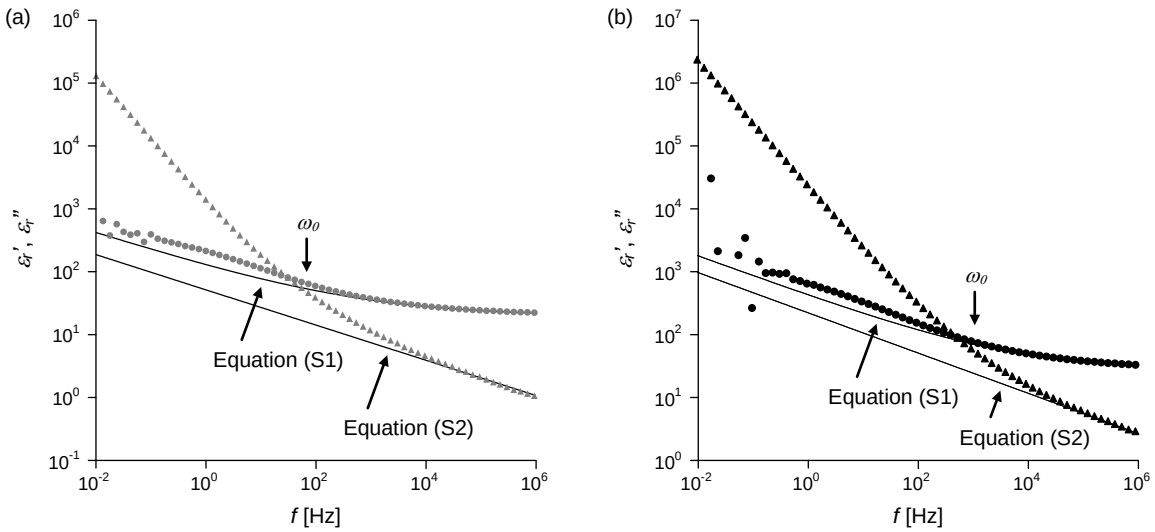

Fig. S6 Comparison between the experimental and theoretical spectra. (a) PCHMA/CNT-Br with Φ_{CNT} = 0.055. (b) PCHMA-CNT with Φ_{CNT} = 0.14. The solid lines are the theoretical curves, eqns (S1) and (S2).

Mechanism of the increase in ε_r' in the polymer/CNT system.

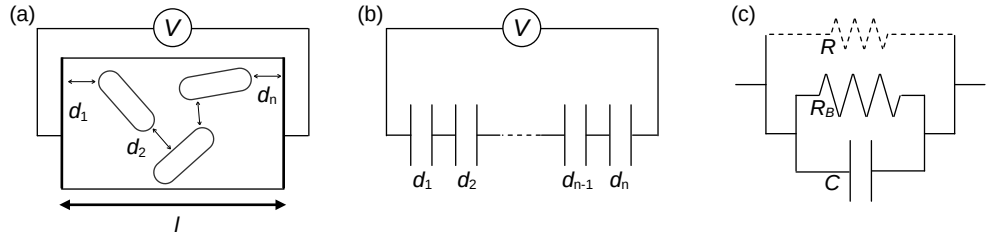

Fig. S7 (a) Schematic of microcapacitors formed between CNTs. d is the internanotube distance (the gap width of the microcapacitor). (b) An electric circuit composed of serially-connected capacitors in disregard of resistances. (c) An imaginary equivalent electric circuit composed of the resistance R, the bulk resistance R_B and the capacitance C for the polymer/CNT composite system. R that is related to the tunneling resistance, can be ignored at the higher frequencies than ω_0 shown in Table 1.

We consider the capacitance for a small area δS of a polymer sample with a thickness l. The capacitance for a neat polymer sample C_B is calculated as:

$$C_B = \varepsilon_r'\varepsilon_0\delta S/l, \quad \text{(S3)}$$

where ε_r' is the dielectric constant of the neat polymer. On the other hand, a polymer/CNT composite sample can be schematically drawn as shown in Fig. S7a. Because the CNT is much higher polarizability than the polymer matrix, the equivalent electric circuit is modeled as only the microcapacitors connected in a series as shown in Fig. S7b: the CNT is simply regarded as a lead of the electric circuit owing to the high conductivity. In the case of n capacitors connected in a series, the total capacitance C_{total} is calculated as:

$$1/C_{total} = 1/C_1 + 1/C_2 \cdots + 1/C_n. \quad \text{(S4)}$$

Therefore, the capacitance for the composite sample C_C is calculated as:

$$C_C = \varepsilon_r'\varepsilon_0\delta S/\Sigma d, \quad \text{(S5)}$$

where δS is a small area of the microcapacitor. If the sum of d is smaller than the sample thickness ($\Sigma d < l$), an apparent increase in the capacitance of the composite sample is concluded ($C_C > C_B$). In the polymer/CNT nanocomposite system, Σd is always much smaller than l because of the high aspect ratio of the CNT. In addition, when some of the microcapacitors are connected by the tunneling conduction, Σd becomes smaller, resulting in

the further increase in the capacitance. It is important that the overall capacitance in a polymer composite system is strongly governed by the matrix component, mostly the polymer with a low dielectric constant, according to the serial capacitance model (eqn S4). Also, one can understand that the applied electric-field to the polymer between the CNTs is enhanced by the incorporation of the CNT as $V/\Sigma d > V/l$, where V is an applied voltage to the sample. This is because almost no electric field is applied to the CNT owing to much higher polarizability. This locally enhancement of the electric-field would be the exact reason for the apparent increase in C_C. Similar field enhancement in composite materials have been demonstrated using simulated methods.[2,3]

2 H. Cheng, S. Torquato, *Phys. Rev. B*, 1997, **56**, 8060.

3 J. Y. Li, C. Huang, Q. Zhang, *Appl. Phys. Lett.*, 2004, **84**, 3124.